Electromagnetic Design Characterization of a Dual Rotor Axial Flux Motor for Electric Aircraft

Dorsa Talebi
Dept. of Elec. & Comp. Engr.
Texas A&M University
College Station, TX, USA
dorsa.talebi@tamu.edu

Matthew C. Gardner
Dept. of Elec. & Comp. Engr.
University of Texas at Dallas
Richardson, TX, USA
Matthew.Gardner@utdallas.edu

Sri Vignesh Sankarraman
Dept. of Elec. & Comp. Engr.
University of Texas at Dallas
Richardson, TX, USA
SriVignesh.Sankarraman@utdallas.edu

Ahmad Daniar
Dept. of Elec. & Comp. Engr.
University of Texas at Dallas
Richardson, TX, USA
Ahmad.Daniar@utdallas.edu

Hamid A. Toliyat
Dept. of Elec. & Comp. Engr.
Texas A&M University
College Station, TX, USA
toliyat@tamu.edu

***Abstract*— This paper presents and evaluates a dual rotor axial flux permanent magnet motor for electric aircraft applications. Several features, including grain oriented electrical steel (GOES), magnet segmentation, and wires with rectangular cross-sections, are used to improve torque density and efficiency. Rather than simply optimizing the motor by itself, this paper evaluates the tradeoffs between motor performance and its interfaces with the drive, thermal management system (TMS), and mechanical structure. This information can be used along with similar analyses of the drive, TMS, and structure to select a design that achieves the system-level optimal performance. The paper uses finite element simulations to characterize tradeoffs between active mass, efficiency, fundamental frequency, power factor, axial forces on the rotors, and cooling surface area. Several designs exceed 95% efficiency at takeoff with less than 8 kg of active mass. While high pole counts, a large outer radius, and short stator teeth tend to optimize the magnetic performance at takeoff, this can reduce cruise efficiency, reduce the surface area through which the TMS can extract heat, increase the fundamental frequency the drive must supply, and increase the structural mass required to support the rotors. Additionally, designs with 20 °C cooler magnets were simulated to evaluate the impact of a more effective TMS, but the improvements in magnetic performance were relatively small.**

Keywords*— *Axial flux PM machine, dual rotor, grain oriented electrical steel, segmented Halbach array, yokeless and segmented armature (YASA), rectangular wire, co-design, slot/pole combination, fractional-slot concentrated windings, finite element analysis, electric aircraft

I. INTRODUCTION

Pure electric and hybrid electric aviation require the weight of the motor, drive, and associated cooling to be minimized [1], [2]. Thus, the US Advanced Research Projects Agency-Energy (ARPA-E) aviation-class synergistically cooled electric motors with integrated drives (ASCEND) program promotes a highly efficient, ultra-lightweight motor, drive, and thermal management system (TMS) for aircraft propulsion with targets listed in Table I [3]. The 12 kW/kg at 5000 RPM target specific power (including motor, drive, and TMS) must be sustained for a minute and gradually ramped down over 20 minutes, as shown in Fig.1. This represents a significant improvement over the state-of-the-art 5 kW/kg aviation motor built by Siemens [4]. Achieving this target will require aggressive designs with tight integration and co-design of the different subsystems and physics.

For this project, an axial flux permanent magnet (AFPM) motor, which is illustrated in Fig. 2, is proposed with several features to achieve a high torque density and a target of 95% efficiency at the peak power. The yokeless and segmented armature (YASA) topology has demonstrated high performance with high current densities [5], which will be

TABLE I. ASCEND PROGRAM SYSTEM TARGETS [3]

Takeoff mechanical shaft power output	≥ 250 kW
Maximum rotational speed at takeoff	5,000 RPM
Specific power at takeoff and climb	≥ 12 kW/kg
Takeoff and climb average efficiency	≥ 93%
Cruise mechanical shaft power output	≥ 83 kW
Cruise rotational speed	3,500 RPM – 4,500 RPM
Average cruise efficiency	≥ 93%

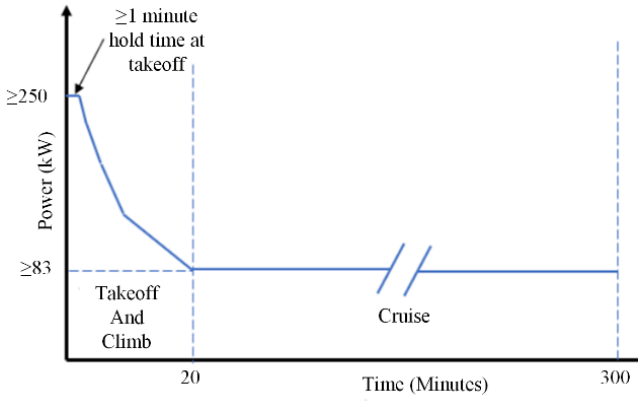

Fig. 1. ARPA-E ASCEND requirement for mechanical power as a function of time flight profile [3].

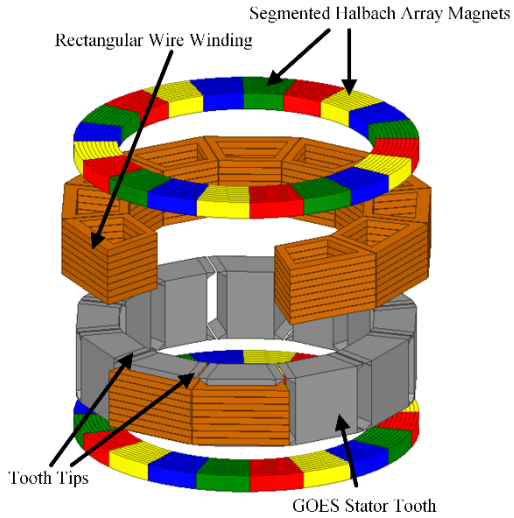

Fig. 2. Exploded view of the motor topology with 12 slots and 5 pole pairs.

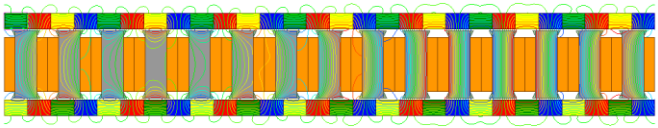

Fig. 3. 2D flux lines distribution of a symmetrical fraction of an example "unrolled" motor design with 30 slots and 14 pole pairs.

required for takeoff. The use of a segmented armature along with the fractional slot concentrated winding facilitates higher slot fill factors [5], [6]. Moreover, the fractional slot concentrated winding (FSCW) configuration improves phase independence and fault tolerance [5]. The shorter end windings in the YASA topology improve the torque density of the motor [6], [7]. Additionally, this topology reduces core losses by replacing the stator yoke with an additional rotor [5], [8], [9]. Grain-oriented electrical steel (GOES) is employed for the stator teeth, which primarily experience axially directed flux in the YASA topology. GOES has a higher permeability and lower losses than non-oriented electrical steel for flux in the direction of the grain [10], [11]. Thus, YASA motors with GOES stators can achieve an extremely high efficiency [10]. The rotor magnets are arranged in a Halbach array to provide a more sinusoidal flux distribution, which can reduce core losses and cogging torque [12]. Additionally, the Halbach array provides a return path for magnet flux [13], allowing the rotor back irons to be replaced with a lightweight carbon fiber reinforced polymer. Fig. 3, which illustrates the flux paths in an "unrolled" 2D model of an example design, demonstrates the significantly reduced leakage flux axially beyond the motor. The permanent magnets are segmented to reduce eddy current losses [14]. Tooth tips also reduce eddy current losses in the magnets and windings and smooth the airgap surface, which results a more sinusoidal airgap flux density. Wires with rectangular cross-sections provide a higher copper fill factor than conventional round wires, which can increase power densities and reduce losses [15], [16]. Furthermore, the YASA topology has two air-gaps, which reduces the stator inductances relative to other topologies and can improve the power factor (PF) [17].

The first step in the co-design process is to characterize each of the subsystems throughout the design space so that a design can be selected for optimal system-level performance. Thus, rather than simply optimizing the motor design, this paper focuses on characterizing the motor's electromagnetic performance, identifying tradeoffs that will affect both the motor and another subsystem (eg. drive or TMS), and quantifying the impacts of these tradeoffs on motor performance. For example, the number of poles affects the electromagnetic performance of the motor and the fundamental frequency of the drive. As another example, the outer surface area of the end windings is the primary area through which the TMS must remove heat from the motor and depends on motor design parameters, such as the stator axial length and the outer radius. Additionally, this paper evaluates many different slot/pole combinations while allowing the geometry to vary, in order to characterize their achievable performances.

II. Design Study Methodology

In general, the FSCW configuration has the advantages of a high slot fill factor and short end windings, but it tends to produce additional spatial harmonics, which can result in significant rotor PM losses [18]. Therefore, there have been studies on pole counts and stator slot counts to find the optimal combinations for key performance indices, such as fundamental winding factor and periodicity, which were verified by finite element analysis (FEA) [19], [20]. In an AFPM motor, the presence of symmetry (periodicity > 1) cancels out the off-axis torques on the rotor to prevent significant noise and vibration [21]. Table II lists several viable, high-performance slot/pole pair (PP) combinations for tooth-wound motors. In this paper, designs with these different slot/PP combinations are evaluated using 3D FEA. (The 3D FEA models have previously been validated against experimental results for a YASA motor with GOES, which is illustrated in Fig. 4 [10].). However, unlike previous studies [19], [20], the machine's geometric parameters, whose values are presented in Table III, are also swept for each slot/PP combination to better compare the achievable performance with each slot/PP combination, as the optimal geometric parameters may depend on the slot/PP combination. Magnetostatic simulations with fixed RMS current densities (29.7 A/mm^2 and 35.6 A/mm^2) were used for the initial analysis to assess which designs might achieve the peak takeoff requirements. These high current densities will only be

TABLE II. Slot/Pole Pair Combinations

Slots/PP	Fundamental winding factor	Periodicity
12/5	0.933	2
18/8	0.945	2
24/10	0.933	4
24/11	0.949	2
24/14	0.933	4
27/12	0.945	3
30/14	0.951	2
36/16	0.945	4
36/17	0.953	2
42/20	0.953	2
45/24	0.951	3
48/26	0.9495	4

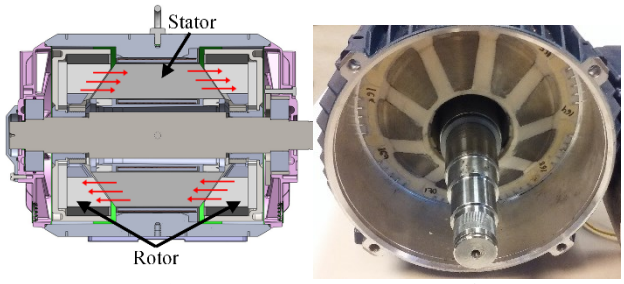

(a) (b)

Fig. 4. (a) Transverse-section (with red arrows illustrating flux direction) and (b) prototype stator of YASA motor with GOES in [10] used to validate FEA models.

TABLE III. PARAMETERS FOR INITIAL MAGNETOSTATIC SIMULATIONS

Name	Description	Values	Units
R_{2S}	Stator Teeth Outer Radius	120,135	mm
R_{1S}	Stator Teeth Inner Radius		
	For R_{2S} = 120	80,85,90,95	mm
	For R_{2S} = 135	100,105,110,115	mm
L_S	Stator Teeth Axial Length		
	For R_{2S} = 120	35,40,45,50	mm
	For R_{2S} = 135	25,30,35,40	mm
FF_{Cu}	Copper Fill Factor	0.8	
k_{tw}	Tooth Width to Tooth Pitch Ratio	0.4,0.5,0.6	
J	RMS Current Density	29.7, 35.6	A/mm^2
A_g	Airgap Thickness	1	mm
L_{Rotor}	Magnet Axial Thickness	5,10,15,20	mm
ω_t	Takeoff Speed	5000	RPM
ω_c	Cruise Speed	4000	RPM

necessary during the limited takeoff time shown in Fig 1. Additionally, the TMS will aggressively extract heat directly from the inner and outer surfaces of the end windings during takeoff and climb. The current density is interpolated in post-processing to produce the required peak torque of 480 Nm. The wire cross-sections and the number of turns can be selected later to determine the terminal voltages and currents to meet the requirements of the drive. Based on the magnetostatic simulation results, the highest performing

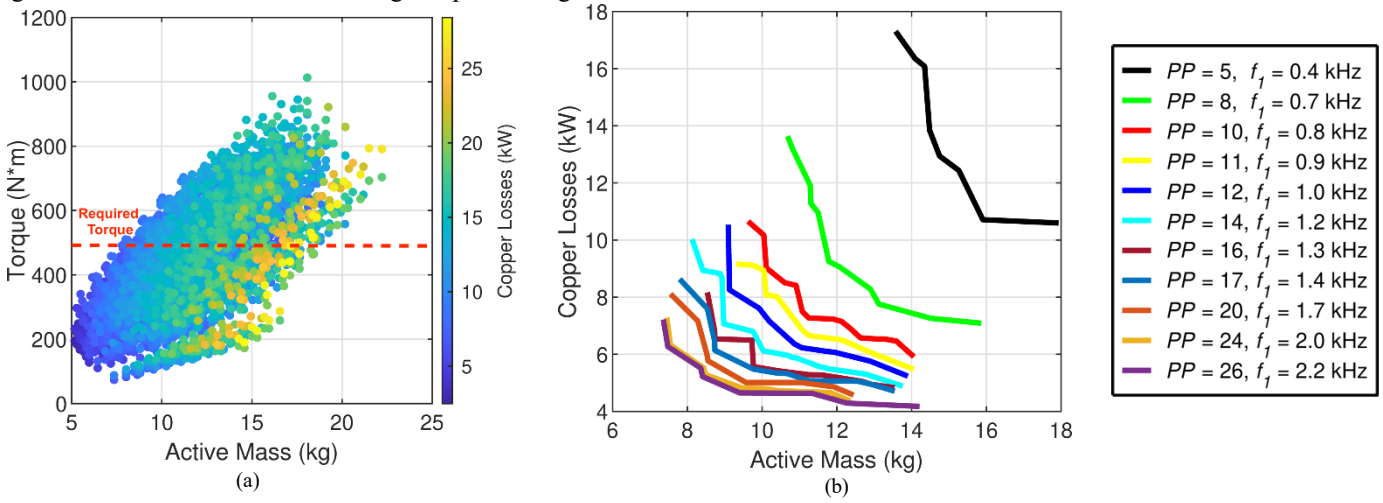

Fig 5. (a) Average torque, copper losses, and total active masses of the simulated cases and (b) Pareto fronts for minimum total active mass and minimum copper losses for different pole pair counts (and, thus, different fundamental frequencies). Only designs with at least 480 Nm of torque are included in Fig. 5(b).

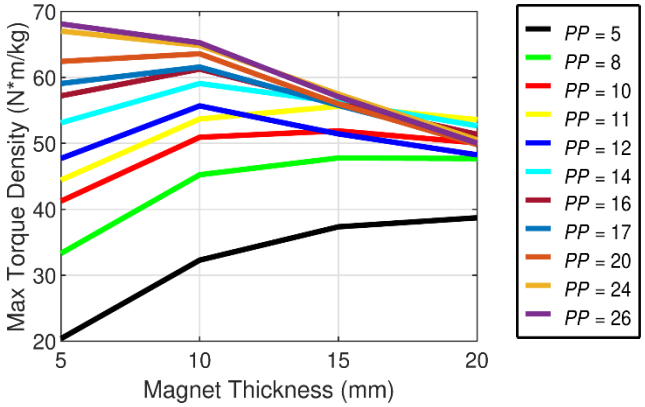

Fig 6. Maximum torque density with different magnet thickness and PP values.

designs were selected, and these designs were evaluated using a transient FEA model to determine core losses and power factor.

III. SIMULATION RESULT

Fig. 5(a) shows the raw (before current density interpolation) magnetostatic simulation results and which cases exceed the required 480 Nm takeoff torque. Fig. 5(b) shows the Pareto front of each PP case for minimizing the total active mass and copper losses based on the Table III design parameters. Fig. 5(b) only includes points which produce at least 480 Nm. The overall trend indicates that lower active masses and copper losses are achievable by increasing PP, if the other geometric parameters are allowed to vary.

Fig. 6 shows the achievable active mass torque densities for different rotor magnet axial thicknesses and PP values. Since the Halbach array provides the flux return path (instead of the rotor back iron), designs with fewer PP require thicker magnets, which increases the active mass. Thus, even though there is not a large difference in the fundamental winding factors in Table II, the designs with more poles are able to achieve higher torque densities.

However, increasing PP beyond 24 does not provide a significant improvement due to high leakage flux through the

much shorter paths between adjacent poles. Moreover; increasing PP requires a higher fundamental frequency (f_1) from the drive design perspective and can increase the core losses. Additionally, increasing PP and slots increases the number of magnet pieces and teeth that are needed for assembling the motor, increasing assembly complexity and the complexity of the TMS.

Fig. 7 shows that the designs with a 135 mm stator teeth outer radius can achieve much better performances than the designs with 120 mm stator teeth outer radius. The larger outer radius yields a larger torque arm, which allows the same torque to be produced with less tangential force. Based on these results, designs with a 150 mm stator teeth outer radius were added to the study. However, only slot/PP combinations of 36/17 and 42/20 were evaluated for the 150 mm stator teeth outer radius, as these combinations represent a compromise between improved performance and avoiding excessive complexity. Table IV summarizes these additional designs.

Fig. 8 shows all the designs that achieved the 480 Nm takeoff requirement with less than 10 kW of copper losses and 9 kg of active mass. These designs were evaluated with transient models for takeoff and cruise conditions. For the takeoff condition, the current density was determined based on the magnetostatic results. For the cruise condition, the designs were simulated at RMS current densities of 10, 15, and 20 A/mm^2, and the appropriate current density to achieve 200 Nm was interpolated.

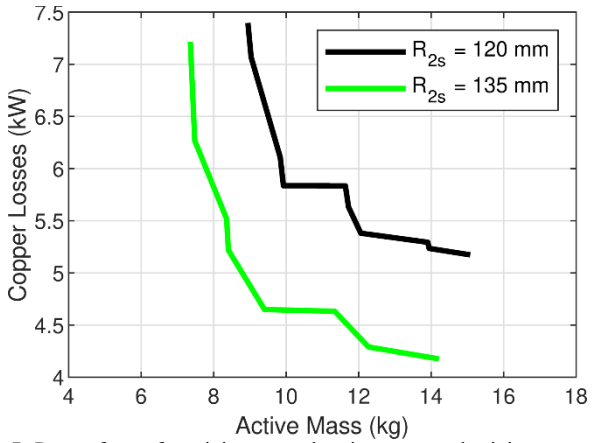

Fig 7. Pareto fronts for minimum total active mass and minimum copper losses for different stator teeth outer radii. Only designs with at least 480 Nm of torque are included.

TABLE IV. ADDITIONAL CASES AT LARGER RADIUS

Name	Description	Values	Units
R_{2S}	Stator Teeth Outer Radius	150	mm
R_{1S}	Stator Teeth Inner Radius	1250, 130, 135	mm
L_S	Stator Teeth Axial Length	20, 25, 30, 35, 40	mm
FF_{Cu}	Copper Fill Factor	0.8	
k_{tw}	Tooth Width to Tooth Pitch Ratio	0.4,0.5,0.6	
J	RMS Current Density	29.7, 35.6	A/mm^2
A_g	Airgap Thickness	1	mm
L_{Rotor}	Magnet Axial Thickness	5,10,15,20	mm
ω_t	Takeoff Speed	5000	RPM
ω_c	Cruise Speed	4000	RPM

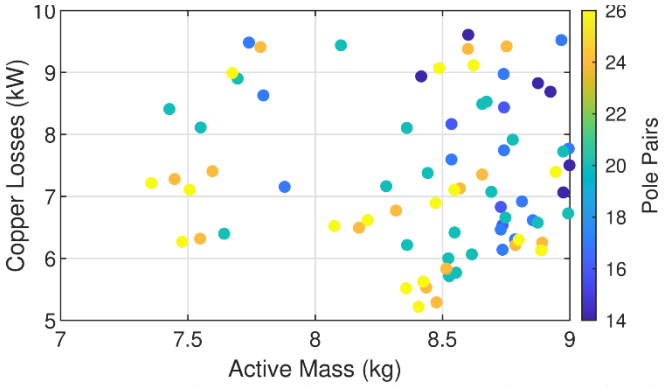

Fig 8. Active mass, takeoff copper losses, and pole pairs of designs selected for transient analysis

Figs. 9(a) and (b) illustrate the efficiencies in takeoff and cruise conditions, respectively. Figs. 10(a) and (b) illustrate what percentage of the electromagnetic losses is from copper loss for each of these designs in takeoff and cruise conditions, respectively. These calculations assume that the losses are dominated by DC copper losses and core losses in the stator laminations. Mechanical losses are neglected, eddy current losses in the magnets are assumed to be small due to magnet segmentation, and AC copper losses are also assumed to be small because the tooth tips shield the windings from the rotor flux. These designs show promising efficiencies at both takeoff (480 Nm, 5000 RPM) and cruise (200 Nm, 4000 RPM) conditions. Fig. 9(a) does not show a strong correlation between PP and efficiency at takeoff; as shown in Fig. 5(b),

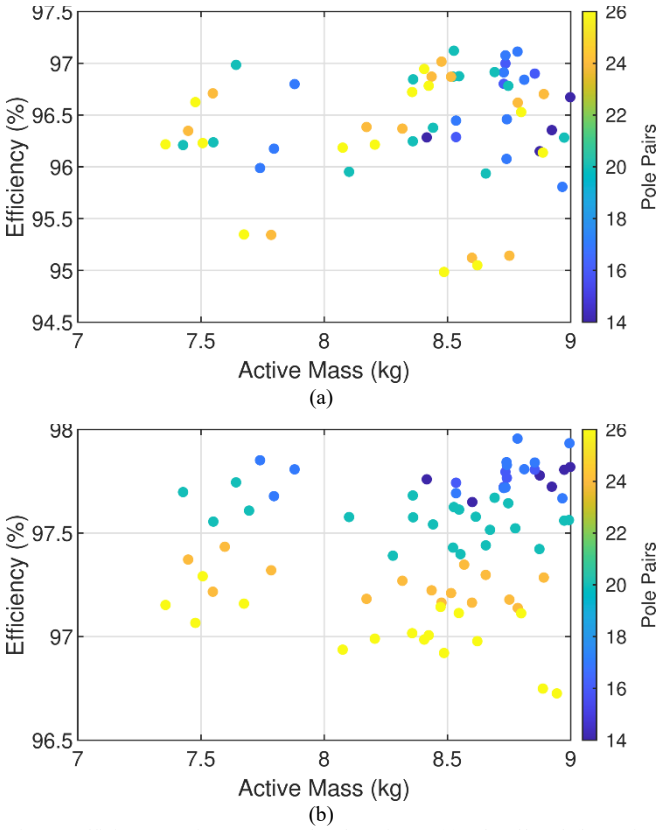

Fig. 9. Efficiency, active mass, and pole pairs at (a) takeoff and (b) cruise conditions.

designs with higher PP can achieve lower copper losses for a given active mass, but these designs also experience higher frequencies, leading to increased core loss densities. Thus, the designs with higher PP tend to have lower copper loss percentages in Fig. 10(a). Fig. 9(b) generally shows higher cruise efficiencies than takeoff efficiencies because the copper losses are dominant at takeoff but decrease quadratically with current density. Additionally, Fig. 9(b) shows a correlation between PP and efficiency. Because the reduced torque at cruise significantly reduces copper losses, the core losses are more significant for all designs, especially those with higher PP, as illustrated in Fig. 10(b).

Fig. 11 illustrates various tradeoffs between active mass, takeoff efficiency, design parameters, and parameters that affect other subsystems (eg. end winding outer surface area). Fig. 11(a) illustrates the tradeoffs between minimizing the active mass, maximizing the efficiency, and maximizing the outer surface area of the end windings. The designs with the lowest masses and highest efficiencies tend to have less end winding surface area. However, the designs with higher efficiency may require less end winding surface area because the TMS will not need to remove as much heat. Fig. 11(b) shows the axial force on the rotors of each design at the takeoff condition. The larger the axial forces, the heavier the rotor support system will need to be, increasing the total (active plus inactive structural) mass of the motor. Fig. 11(c) shows the

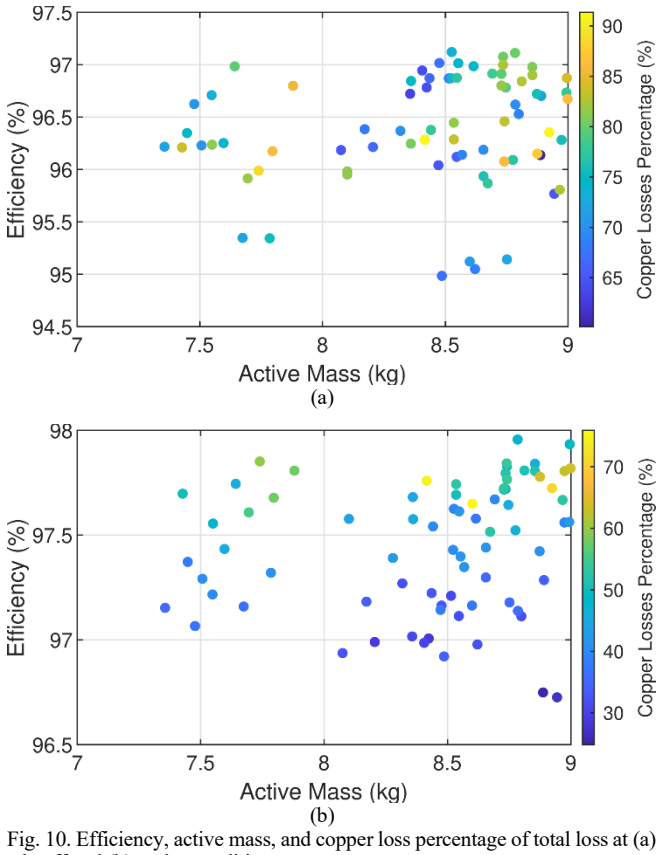

Fig. 10. Efficiency, active mass, and copper loss percentage of total loss at (a) takeoff and (b) cruise conditions.

current densities of each of the designs at the takeoff condition. The designs with the very smallest active masses tend to have current densities near the upper limit so that they can produce the most torque with the least active material. However, the designs with the very highest efficiencies tend to have lower current densities because the copper loss density scales with the square of the current density.

Figs. 11(d)-(h) show various geometric parameters, and Fig. 11(i) shows the surface area of an airgap for each of the designs. The axial forces are strongly correlated with the magnet thicknesses and airgap surface areas; increasing either the magnet thickness or the air gap surface area tends to increase the axial forces on the rotors. Fig. 11(d) shows that the 25 mm and 30 mm stator axial length designs are electromagnetically optimal; the designs with larger stator axial lengths tend to be heavier and less efficient. On the other hand, none of the designs with a 150 mm stator teeth outer radius and 20 mm stator axial length achieved the target torque with acceptable mass and losses. However, increasing the stator length increases the end winding surface area, which can facilitate better cooling. Additionally, the designs with longer stator lengths tend to have thinner magnets or reduced airgap surface areas, decreasing the axial forces on the rotors. Fig. 11(e) shows that the optimal magnet thickness is near 10 mm. The designs with 15 mm or 20 mm thick magnets are too heavy, whereas the designs with 5 mm thick magnets tend to be less efficient because more amp-turns are required to produce the necessary torque. Fig. 11(f) shows that the optimal designs have a tooth width to tooth pitch ratio of 0.4, meaning that the stator slots are tangentially wider than the stator teeth. Increasing k_{tw} increases the surface area of the tooth, potentially allowing more flux to pass through the stator. However, increasing k_{tw} also reduces the slot width and requires an increase in stator length, airgap surface area, or current density to achieve the required torque. Increasing stator length or airgap surface area increases the active mass, whereas increasing current density increases the copper loss density. Fig. 11(g) shows that the smallest outer radius considered did not yield adequate performance. Increasing the stator teeth outer radius to 150 mm allows the radial thickness or axial length of the stator teeth to decrease, but this does not reduce the active mass as much as going from 120 mm to 135 mm for the stator teeth outer radius. However, the larger outer radius for the stator teeth results in a larger outer radius for the magnets, which can make the mass of the rotor support structure larger.

Figs. 12(a) and (b) present the approximate PF in takeoff and cruise conditions, respectively. In this calculation, the PF is estimated for max torque per amp (MTPA) operation from the back emf coefficient and the apparent inductances. Fig. 12(a) shows that the designs with higher takeoff efficiencies tend to have higher PF. The designs with lower efficiencies will tend to have higher copper losses, correlating to having more amp-turns, or higher core losses, due to higher fundamental frequencies or higher stator teeth volumes. Increasing the stator teeth volume will tend to increase the inductances. Thus, the designs with lower takeoff efficiencies tend to have more reactive power at takeoff. However, Fig. 12(b) shows that when the currents are significantly decreased in cruise mode, all the designs have high PF in MTPA operation, due to the relatively low inductance of the YASA topology [17].

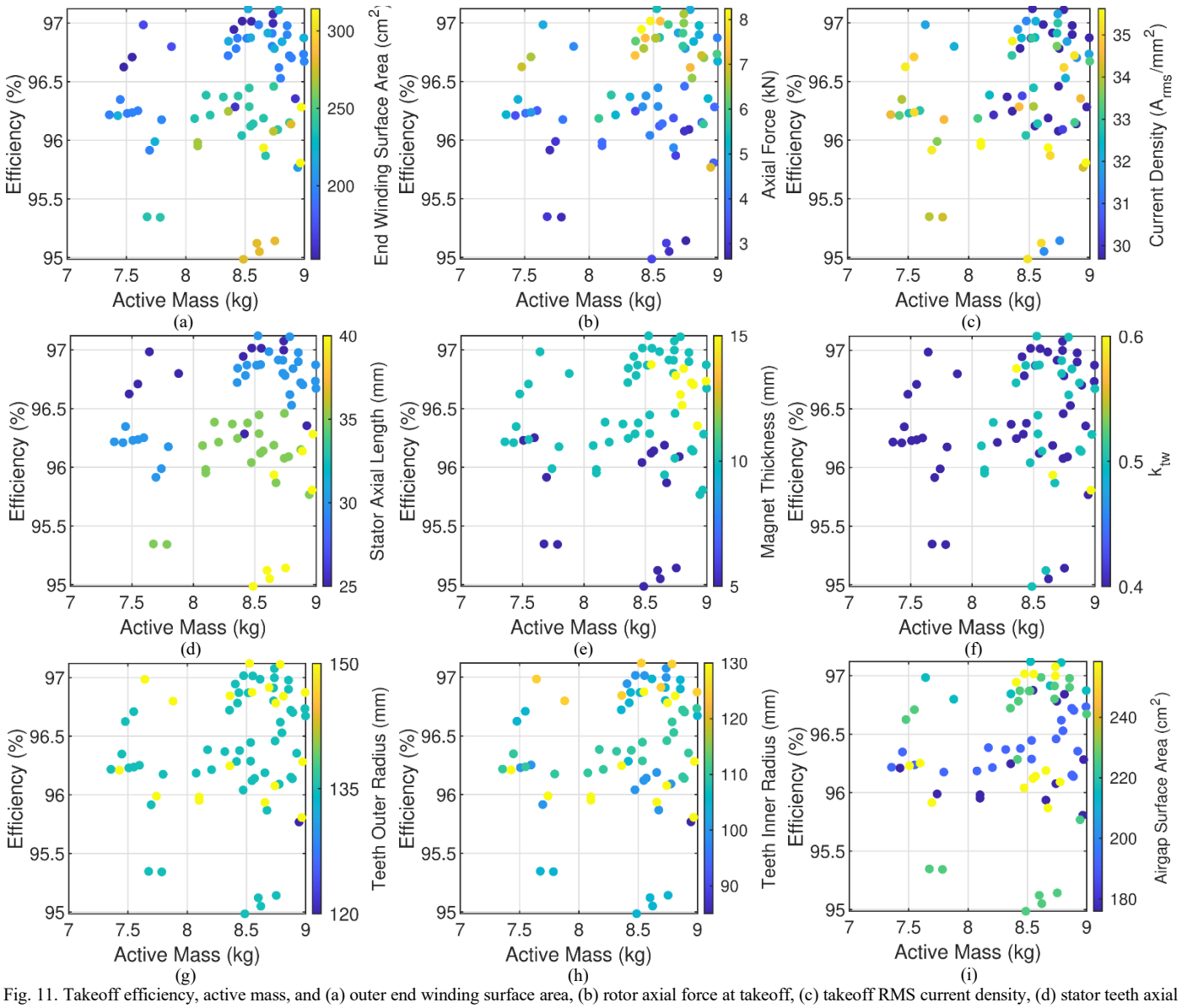

Fig. 11. Takeoff efficiency, active mass, and (a) outer end winding surface area, (b) rotor axial force at takeoff, (c) takeoff RMS current density, (d) stator teeth axial length, (e) magnet axial thickness, (f) tooth width to tooth pitch ratio, (g) stator teeth outer radius, (h) stator teeth inner radius, or (i) surface area of an airgap for the designs evaluated with transient simulations.

While the previous results are based on a magnet temperature of 100 °C, more aggressive cooling could potentially keep the magnets at a lower temperature. Thus, similar magnetostatic simulations were run for magnet temperatures of 80 °C. Fig. 13 compares the Pareto fronts for the simulations at the two temperatures for some pole pair counts. Fig. 13 shows a relatively minor reduction in active mass and copper losses. However, a slightly more significant improvement might be achieved if the reduced temperature allowed a higher magnet grade to be used without being demagnetized.

IV. Conclusion

This paper evaluates a YASA motor with segmented Halbach array magnets, rectangular wires, and grain oriented electrical steel for an electric aircraft propulsion application. Because the electric aircraft requires the mass and efficiency of the entire drivetrain to be optimized, the motor must be tightly integrated and codesigned with the drive and thermal management system. This paper addresses the first step of this optimization for the motor, which is to characterize its electromagnetic performance throughout the potential design space. The results show that the motor can achieve the necessary torque for takeoff with less than 8 kg of active mass and electromagnetic efficiencies greater than 95%. This analysis also identifies tradeoffs between motor performance and the motor's interface with the other systems and characterizes those tradeoffs and which parameters drive those tradeoffs.

The current density contributes to the tradeoff between active mass and efficiency. The minimum active mass designs tend to have higher current densities, whereas the maximum efficiency designs tend to have lower current densities.

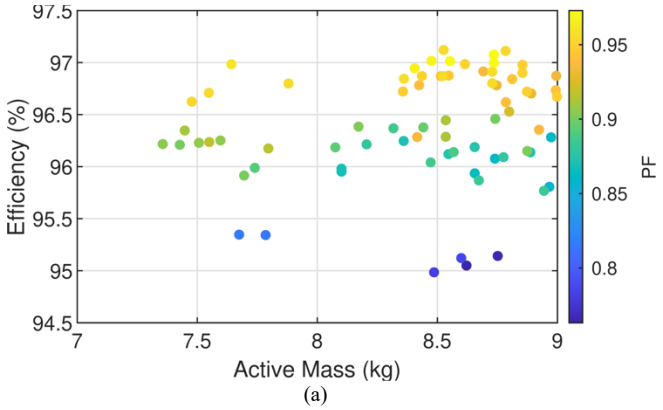

Fig. 12 Efficiency, active mass, and PF at (a) takeoff and (b) cruise conditions for MTPA operation.

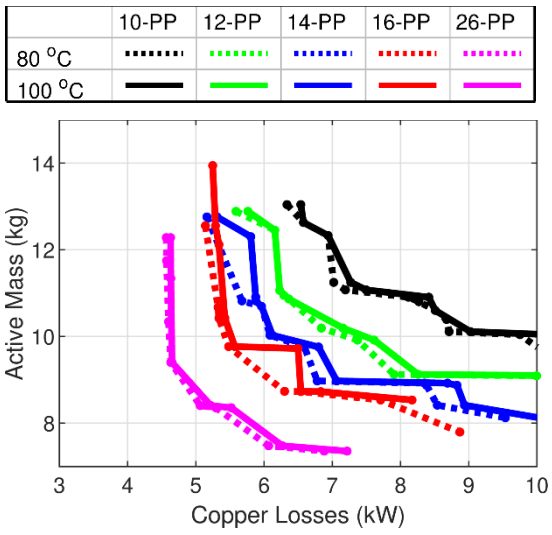

Fig. 13. Pareto optimal fronts for minimizing active mass and copper losses for different pole counts assuming 80 °C or 100 °C magnet temperature.

While a large number of pole pairs increases the fundamental frequency that the drive must supply, it can reduce the active mass and copper losses of the motor. One reason that this occurs is that lower pole counts require thicker magnets in the Halbach array for the flux return path in the rotor. However, increasing the number of pole pairs increases the motor and TMS complexity. Additionally, increasing the number of pole pairs increases the core losses; thus, designs with higher pole counts achieved comparable takeoff efficiencies to designs with lower pole counts. However, during cruise conditions, the designs with higher pole counts achieved lower efficiencies because the core losses contributed a larger percentage of the electromagnetic losses than during takeoff.

The outer radius provides another tradeoff. Increasing the outer radius can improve electromagnetic performance, but it will also increase the amount of material required to mechanically support the rotor.

The axial forces on the rotors are largely driven by the magnet thickness and the airgap surface area. Thus, designs with larger stator teeth lengths and reduced airgap surface areas or reduced magnet thicknesses can require less rotor support material. Additionally, increasing the stator teeth length tends to increase the end winding surface area, which can facilitate better heat extraction from the windings.

Generally, the magnetic performance can be improved by using a high number of pole pairs, a large outer radius, and short stator teeth. However, such a design does not necessarily yield the optimal system-level performance. Reducing the number of pole pairs can reduce complexity and improve cruise efficiency. Using longer stator teeth with a smaller airgap surface area can increase the end winding surface area, facilitating better cooling, and reduce the axial forces on the rotors, reducing the required structural mass.

ACKNOWLEDGMENT

Portions of this research were conducted with the advanced computing resources provided by Texas A&M High Performance Research Computing. The authors would like to thank ANSYS for their support of the EMPE lab through the provision of FEA software.

REFERENCES

[1] B. Sarlioglu and C. T. Morris, "More electric aircraft: review, challenges, and opportunities for commercial transport aircraft" *IEEE Trans. Transport. Electrific*., vol. 1, no. 1, pp. 54-64, Jun. 2015.

[2] F. Kelch, Y. Yang, B. Bilgin, and A. Emadi, "Investigation and design of an axial flux permanent magnet machine for a commercial midsize aircraft electric taxiing system," *IET Electr. Syst. Transp*., vol. 8, no. 1, pp. 52-60, Mar. 2018.

[3] "DE-FOA-0002238: Aviation-class synergistically cooled electric-motors with integrated drives (ASCEND)", Department of Energy, Advanced Research Projects Agency Energy, Dec. 16, 2019.

[4] "Siemens develops world-record electric motor for aircraft," Siemans, Mar 2015, Press. [Online]. Available: https://press.siemens.com/global/en/pressrelease/ siemens-develops-world-record-electric-motor-aircraft.

[5] N. Taran, G. Heins, V. Rallabandi, D. Patterson, and D. M. Ionel, "Evaluating the effects of electric and magnetic loading on the performance of single- and double-Rotor axial-flux PM machines," *IEEE Trans. Ind. Appl*, vol. 56, no. 4, pp. 3488-3497, Jul.-Aug. 2020.

[6] B. Zhang, Y. Wang, M. Doppelbauer and M. Gregor, "Mechanical construction and analysis of an axial flux segmented armature torus machine," in *Proc. IEEE Int. Conf. Elect. Mach.*, 2014, pp. 1293-1299,

[7] P. Ojaghlu and A. Vahedi, "A New Axial Flux Permanent Magnet Machine," *IEEE Trans. Magn*., vol. 54, no. 1, pp. 1-6, Jan. 2018

[8] N. Taran, G. Heins, V. Rallabandi, D. Patterson, and D. M. Ionel, "Systematic comparison of two axial flux pm machine topologies: Yokeless and segmented armature versus single sided", in *Proc. IEEE Energy Convers. Congr. Expo*, 2019, pp. 4477-4482.

[9] T.J. Woolmer, M.D. McCulloch, " Analysis of the yokeless and segmented armature machine", in *Proc. IEEE Int. Elect. Mach. Drives Conf.*, 2007, pp. 704-708.

[10] M. C. Gardner, Y. Zhang, D. Talebi, H. A. Toliyat, A. Crapo, P. Knauer, and H. Willis, "Loss Breakdown of a Dual Conical Rotor Permanent Magnet Motor using Grain Oriented Electrical Steel and Soft Magnetic Composites", in *Proc. IEEE Int. Elect. Mach. and Drives Conf*., 2019, pp. 1067-1074.

[11] D. Kowal, P. Sergeant, L. Dupr, and A. Van den Bossche, "Comparison of nonoriented and grain-oriented material in an axial flux permanent-magnet machine", *IEEE Trans. Magn*., vol. 46, no. 2, pp. 279-285, Feb. 2010.

[12] Z. Q. Zhu and D. Howe, "Halbach permanent magnet machines and applications: A review", *IEE Proc.-Elect. Power Appl*., vol. 148, no. 4, pp. 299-308, Jul. 2001.

[13] M. Johnson, M. C. Gardner, and H. Toliyat, "Analysis of axial field magnetic gears with Halbach arrays", in *Proc. IEEE Int. Elect. Mach. Drives Conf*., 2015, pp. 108-114.

[14] P. Sergeant and A. van den Bossche, "Segmentation of Magnets to Reduce Losses in Permanent-Magnet Synchronous Machines", *IEEE Trans. Magn*, vol. 44 no. 11, pp. 4409-4412, Nov. 2008.

[15] Y. Zhao, D. Li, T. Pei, and R. Qu, "Overview of the Rectangular Wire Windings AC Electrical Machine", *CES Trans. Elect. Mach Syst*, vol. 3, no. 2, pp. 160-169, Jun. 2019.

[16] J. H. Choi., Y. D. Chun, P. W. Han, M. J. Kim, D. H. Koo, J. Lee, and J. S. Chun, "Design of high power permanent magnet motor with segment rectangular copper wire and closed slot opening on electric vehicles", *IEEE Trans. Magn.*, vol. 46, no. 6, pp. 2070-2073, Jun. 2010.

[17] D. Winterborne, N. Stannard, L. Sjöberg and G. Atkinson, "An Air-Cooled YASA Motor for in-Wheel Electric Vehicle Applications," IEEE Trans. Ind. Appl., vol. 56, no. 6, pp. 6448-6455, Nov.-Dec. 2020.

[18] A. M. El-Refaie, "Fractional–slot concentrated–windings synchronous permanent magnet machines: opportunities and challenges", *IEEE Trans. Ind. Electron.*, vol. 57, no. 1, pp. 107-121, Jan. 2010.

[19] P. Ponomarev, P. Lindh, and J. Pyrhönen, "Effect of Slot-and-Pole Combination on the Leakage Inductance and the Performance of Tooth-Coil Permanent-Magnet Synchronous Machines", *IEEE Trans. Ind. Electron.*, vol. 60, no. 10, pp. 4310-4317, Oct. 2013.

[20] S. Skoog and A. Acquaviva, "Pole-slot selection considerations for double layer three-phase tooth-coil wound electrical machines", in *Proc. IEEE Int. Conf. Elect. Mach.*, 2018, pp. 934-940.

[21] A. Cavagnino, M. Lazzari, F. Profumo, and A. Tenconi, "A comparison between the axial flux and the radial flux structures for PM synchronous motors", *IEEE Trans. Ind. Appl.*, vol. 38, no. 6, pp. 1517-1524, Nov.-Dec. 2002.